Cytotherapy 28 (2026) 102034

Contents lists available at ScienceDirect

FULL LENGTH ARTICLE

CYTOTHERAPY

journal homepage: www.isct-cytotherapy.org

International Society ISCT Cell & Gene Therapy®

Process Development and Manufacturing

SMART sensors for cell growth monitoring in closed system G-Rex for scalable, cost-conscious cell and gene therapy manufacturing

Subhanwit Roy[1], Samuel Rothstein[1], Aidan Shervheim[1], Yee Jher Chan[1], Cameron Greenwalt[1], Nathan Neihart[1], Jose Juarez[2], Patricia Turner[2], Andrew Lewis[2], Nathan Dunkerley[2], Dan Welch[3], John Wilson[2,3], Dan Fick[2,3], Nigel F. Reuel[1,*]

[1] Skroot Laboratory Inc., Ames, Iowa, USA
[2] CellReady LLC, Houston, Texas, USA
[3] Wilson Wolf Manufacturing LLC, St. Paul, Minnesota, USA
*Correspondence: Nigel F. Reuel, PhD, 2501 N. Loop Drive, Suite 1000 Ames, IA 50010 USA. *E-mail address:* reuel@skrootlab.com (N.F. Reuel).

A B S T R A C T

Background: Cell and gene-modified cell therapy (CGT) includes creating engineered cancer killing cells *ex vivo* and then subsequently putting them into the patient's body to selectively attack cancerous cells. An immune cell manufacturing device called G-Rex (for "gas permeable rapid expansion"), is widely used for production in current clinical trials and commercially approved drug products. G-Rex is uniquely simple as it eliminates the need for pumps and flow circuits to deliver oxygen and nutrients and instead relies on passive convection, greatly minimizing complexity and allowing for scalable manufacturing. The elimination of the need to pump media allows concurrent manufacturing without requiring additional capital equipment investments, thereby decreasing cycle times and increasing utilization rates of existing equipment and space. To further simplify G-Rex based manufacturing operations, it would be ideal to eliminate any need of physical intervention to assess cell quantity. Alternative CGT drug product manufacturing technologies require invasive sampling of media or cell suspension to determine cell quantity or monitor cell growth characteristics.
Methods: With that goal in mind, herein we describe integration of a "single-use metabolite absorbing resonant transducer" in G-Rex (SMART G-Rex) and an accompanying contact-free reader (SMART Reader). The SMART G-Rex is wirelessly interrogated by the SMART Reader to determine the extent of cell expansion in the G-Rex at any given time. As cell quantity increases, the SMART G-Rex absorbs cell secreted metabolites (organic compounds such as eicosanoids) which cause a change in resonant frequency (measured as % of frequency change, or Skroot Growth Index (SGI)).
Results: Results: By placing SMART G-Rex in proximity of the SMART Reader, whether in or out of an incubator, changes in resonant frequency are detected and translated into cell quantity with high reliability (<1.5% coefficient of variation across replicates). For example, using 45 sensors across multiple donor cell samples, we established 99% confidence in the SMART system's accuracy at signaling a >60X expansion (3×10^9 viable cells) at harvest. Benchtop reader measurements required approximately 15 minutes to read 11 vessels (average of 1 minute 20 seconds per vessel), representing a >50% reduction in time compared to conventional manual sampling and a complete elimination of invasive sampling altogether.
Conclusions: The SMART G-Rex provides a rapid, noninvasive, and scalable means for real-time quantification of the viable cell count in a CGT drug production process and informs manufacturers when a CGT drug product has reached the desired quantity of cells necessary to proceed with formulation, fill, and finish.

Key Words: cell expansion, cell quantification, contact free, process analytical technologies (PAT), static bioreactor.

Introduction

Personalized cell therapies are opening a new epoch in drug development [1]. Chimeric antigen receptor T (CAR-T) cell therapies, in which a patient's T-cells are genetically engineered to express a CAR that is designed to recognize specific tumor targets, have become mainstream cancer treatments [2]. Seven CAR-T drug products are commercially available for leukemia, lymphoma, and myeloma and over 1000 clinical trials are being pursued globally for cancer and more recently for autoimmune diseases [3]. The treatable patient population continues to rise. One estimate identified 450 000 eligible patients in 2019, with projected growth to 2 million in 2029 [4]. But the capacity to manufacture drug products for this number of people is in question. Manufacturing limitations are made clear by the fact

https://doi.org/10.1016/j.jcyt.2025.102034

that as of 2025, barriers to manufacturing scale out are being reported by commercial drug manufacturers [5–8].

A root cause of manufacturing limitations includes the fact that CAR-T drug products typically originate in academic centers where state-of-the-art manufacturing skills are of little importance compared to knowledge of the mechanisms of action in a drug product that drive safety and efficacy. This results in wide differences in every element of the manufacturing process from drug product to drug product and academic institute to academic institute. As the private sector spins these drug products out of the academic centers for commercialization, the poorly conceived manufacturing processes follow. From there, companies focus on quickly gaining more clinical data, which takes precedent over stopping to improve the manufacturing process. With each company focused on clinical data there has been little focus on standardizing elements of the drug product manufacturing process. Yet, there is ample opportunity to standardize manufacturing because the manufacturing steps of every CGT drug product have much in common [9]. At a minimum, three steps are certain to be present. Cells need oxygen, cells need nutrients, and the quantity of cells needs to be known before manufacturing is terminated to ensure the patient dose requirements are met.

A simple manufacturing platform to provide cells with oxygen and nutrients is called G-Rex which stands for Gas Permeable Rapid Expansion of cells [10]. When cells are in G-Rex, they gravitate through nutrient-containing medium to the bottom of G-Rex where they reside on a highly gas permeable membrane and as cells consume oxygen, they create an oxygen concentration gradient across the gas permeable membrane. In response, oxygen from external air diffuses into G-Rex at the rate cells need it. At the same time, G-Rex holds a large volume of nutrients that feed cells by naturally occurring convective movement.

Another key attribute of G-Rex is that it occupies very little space and can use standard cell culture incubators for temperature and pH control. Absent oxygen and nutrient pumping mechanisms that are inherent to all other forms of CGT drug product manufacturing processes, G-Rex is unencumbered by the space requirements of pumping equipment and about 40 G-Rex devices can occupy a standard cell culture incubator [11]. On the contrary, competing pump-based technology requires its own custom incubator. The net result is that on a space occupancy metric, G-Rex in comparison to pumping systems can produce drug products at a ratio of about 40 patients to just 1. Figure 1 provides a space comparison of G-Rex with a typical system that force feeds cells with oxygen and nutrients (assuming a 215 ft^2 production suite that can serve three pump systems at 18 doses per system annually as described in a recent study [12] vs. 40 G-Rex doses per week in the same space with two standard incubators resulting in 2000 doses annually). This uniquely simple method of oxygenating and feeding cells in G-Rex maximizes the utilization of space, personnel, and equipment which reduces cost of goods sold (COGS). But more importantly, this simple approach to manufacturing allows a level of scalability that is unattainable when cells require additional pumps for oxygen and nutrients. The net result is lowered manufacturing cost and greater patient access.

Despite the advantages of G-Rex for manufacturing CGT drug products, like all other CGT manufacturing technology, it still carries a need for intervention to determine cell quantity. Cells expand best when left undisturbed on the gas permeable membrane, and thus traditional cell counting via resuspension and sample collection is not recommended during the expansion phase in the G-Rex. Instead, the current best practice is to sample the media, leaving the cells undisturbed, and measure the reduction in glucose and/or increase in lactate levels to monitor cell growth progression [13]. This sampling

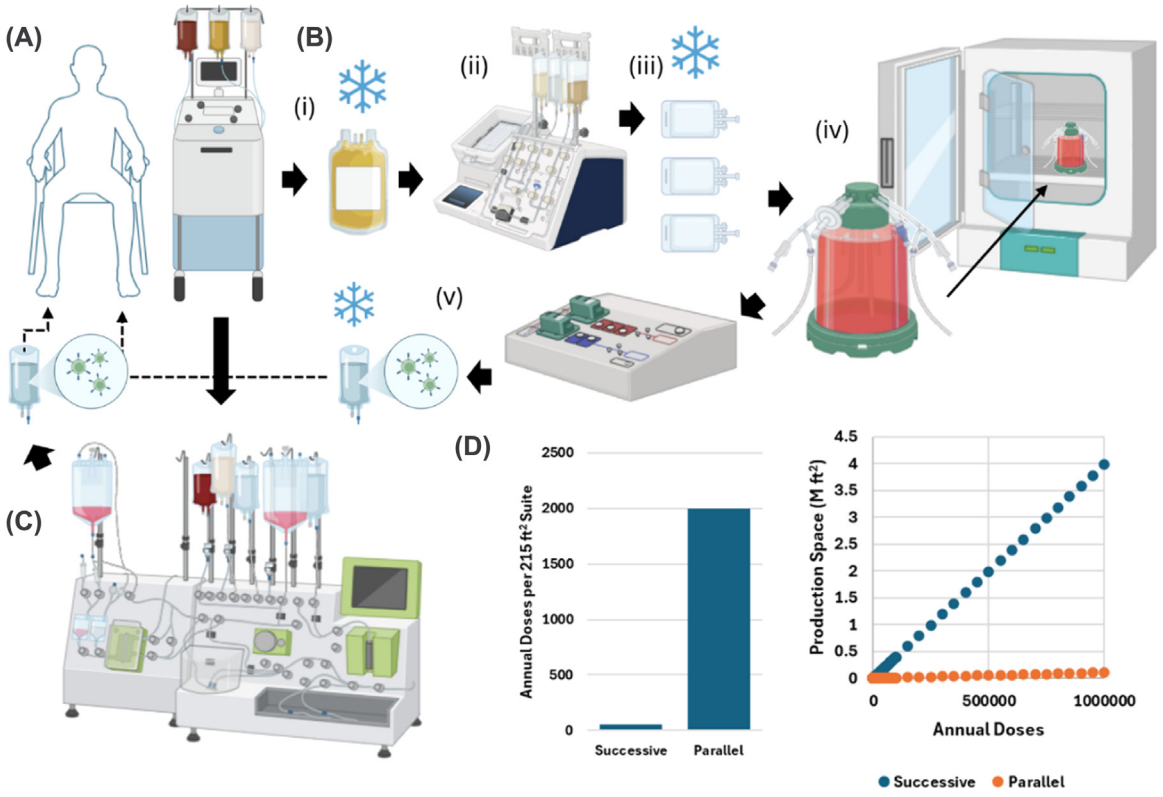

Fig. 1. Comparison of the parallel CAR-T process (assembly line with G-Rex) and successive single dose per unit processes. In both workflows, patient cells are collected and separated via leukapheresis (A). (B) CAR-T production with G-Rex has discrete, parallelizable unit operations: i) frozen leukocytes are thawed; ii) T cells are enriched and then aliquoted (iii) to individual dose size; (iv) these are dosed into G-Rex vessels, activated, transduced, and expanded; (v) cells are then harvested and stored as a patient dose. (C) Illustration of a successive, single dose system, such as the CliniMACS Prodigy, that has limited, serial production. (D) Comparison of annual throughput for both systems and scaling of production floor space required.

methodology requires careful handling of each G-Rex and unique or custom-made consumables to facilitate closed system sampling, or a biosafety cabinet to remove the samples in an open system and then run them through an analyzer, most frequently test strips. Recent efforts have been made to automate or make this media sampling continuous, such as with the integrated MAVEN sensor and an offline analyzer (BioProfile FLEX2, Nova Biomedical) from 908 devices [14]; however, such an approach requires additional tubing, fluid handling pumps, and fluidic sensors for each G-Rex which limits scalability. After expansion is completed (lactate levels plateau) the cells are harvested, and a cell count is used to confirm cell quantities sufficient for patient dosing have been achieved. Each of these hands-on steps contribute to the direct labor costs of the final product. We have discovered a way to eliminate the need for these steps through integration of the SMART sensor.

We now describe the application of single-use metabolite absorbing resonant transducer (SMART) sensor, built into G-Rex, that informs the user of cell quantity without any intervention. The inherent benefit of the SMART sensor as an alternative to human intervention is to reduce direct labor cost, eliminate the risk of contamination, and allow reliable monitoring of cell growth without any need to open the G-Rex or remove from an incubator for such assessment.

Methods

1. Sensor fabrication and testing—Resonant sensors are passive inductor-capacitor (LC) circuits whose measured resonant frequency shifts when the electrical permittivity of their immediate environment changes. Their utility for wireless monitoring in sealed or otherwise nonvented systems (where direct access to the interior is not practical or permitted) has been documented across several application areas [15,16]. In the specific context of cell culture monitoring, they enable noncontact interrogation of cultures without sampling. Recently, an advancement on the conventional resonant sensor called the SMART (single-use, metabolite absorbing resonant transducer) sensor was introduced [17]. The SMART design incorporates a polymer layer that softens in response to secreted metabolites, amplifying the local permittivity contrast above the conventional resonator and providing >20-fold higher sensitivity to growth dynamics than direct resonant sensing. Physically, the SMART sensor comprises five layers (from fluid-facing side to vessel-facing side): a transduction membrane responsive to secondary metabolites, a polyethylene terephthalate (PET) sheet with engineered voids, a bonding interlayer, a patterned LC resonator (copper coil on polyimide), and a mounting adhesive for vessel attachment (Figure 2A) [18].

   As cells grow, secreted secondary metabolites (organic signaling molecules) selectively absorb into the SMART sensor membrane, softening the membrane material such that it partially collapses into engineered voids in the sensor structure (Figure 2B). Prior screening work has shown that simple terpenoids, such as prenol, produce strong responses. For T cells, there is evidence of secreted lipid mediators, including eicosanoid derivatives (e.g., prostanoids and leukotrienes), as signaling molecules [19]. We have verified that arachidonic acid (AA), an omega-6 PUFA that is a precursor to eicosanoids, causes a robust sensor response (Supplement 1). This is representative of a broad class of secreted organic compounds that these cells produce during active growth that act as a plasticizer on the sensor membrane.

   To operationalize the above sensing principle, we fabricated SMART sensors as 2.54 cm x 2.54 cm multilayer laminates comprising the aforementioned five layers. Resonators were produced in array format on polyimide-copper laminate using mask patterning followed by copper etching. Lamination was then performed in two stages to ensure flatness and eliminate trapped air: first the resonator/interlayer/PET stack was aligned and pressed at room temperature under uniform load to ensure consistent bonding, then the transduction membrane was added to the fluid-facing surface, and the assembly was pressed again. Individual sensors were separated by precision cutting. All lamination steps were performed under controlled pressure and dwell time—using a rigid backing plate to maintain uniform layer thickness across the batch.

   A key advancement over prior work was the use of laser-cut PET to define the structured air voids, enabling larger-scale sensor production and greater consistency than previous wire-wound designs. When the transduction membrane softens and the air voids are filled, the growth medium is brought physically closer to the resonator, increasing local permittivity and coil capacitance, which in turn produces a measurable downward shift in resonant frequency. Additionally, increasing the width of the PET air gaps (kerf) emerged as a useful design parameter for tuning sensor sensitivity (Supplement 2).

   To mount the sensor inside the G-Rex vessel, the backing liner of the mounting adhesive was removed, and the sensor was loaded into a custom-designed positioning guide. This guide included alignment features that matched the vessel contour and a mechanical stop to control insertion depth. It ensured that each sensor was positioned at a fixed radial sector and a consistent vertical distance from the gas-permeable membrane, minimizing placement variability across vessels. Once inserted, a soft elastomer stamp was used to press the sensor firmly onto the interior vessel wall, starting from the center and moving outward to eliminate trapped air and ensure full adhesive contact. The applied pressure was gentle but uniform to prevent deformation of the vessel wall or sensor laminate. After sensor placement, the liner protecting the transduction membrane was removed, and the G-Rex was assembled according to Wilson Wolf's standard assembly procedure. The entire sensor application and G-Rex assembly process was performed inside an ISO-5 clean hood to minimize risks of particulates and contamination. The assembled vessels were then inspected visually to confirm proper sensor adhesion and the absence of trapped air bubbles, and each applied sensor's resonant frequency was subsequently probed with a standard vector network analyzer (VNA) for quality control (QC). The SMART G-Rex vessels were then packaged for sterilization by gamma irradiation to ensure sterility prior to cell culture use.

   Sensor consistency was measured by placing replicates (n=4) of the SMART sensor on the same vessel, and determining the coefficient of variation in the sensor response. To assess scalability, sensor fabrication was also outsourced to a flexible circuit manufacturer (Flexible Circuit Technologies) and compared with in-house assembled sensors. The third-party sensors were further subjected to cytotoxicity testing and accelerated aging to determine the robustness of this fabrication method for commercial implementation. Cytotoxicity testing of the sensor mounted within a polycarbonate cap was executed at NAMSA to evaluate for potential cytotoxic effects using an *in vitro* mammalian cell culture test according to ISO 10993-5 and BS EN ISO 10993-5, Biological evaluation of medical devices - Part 5: Tests for in vitro cytotoxicity, whereas accelerated aging was performed at Skroot by placing vessels with attached sensors in a Fisherbrand Oven at 59°C for 4, 8, and 12 weeks to achieve equivalent aging of 1, 2, and 3 years respectively [20], following which cell culture tests were performed at CellReady, LLC to evaluate sensor response of the differently-aged vessels (Supplement 3).
2. Reader design—The original plan for reading the SMART sensors was to use a MetroVNA, a commercially available portable vector network analyzer (VNA). However, initial testing demonstrated a

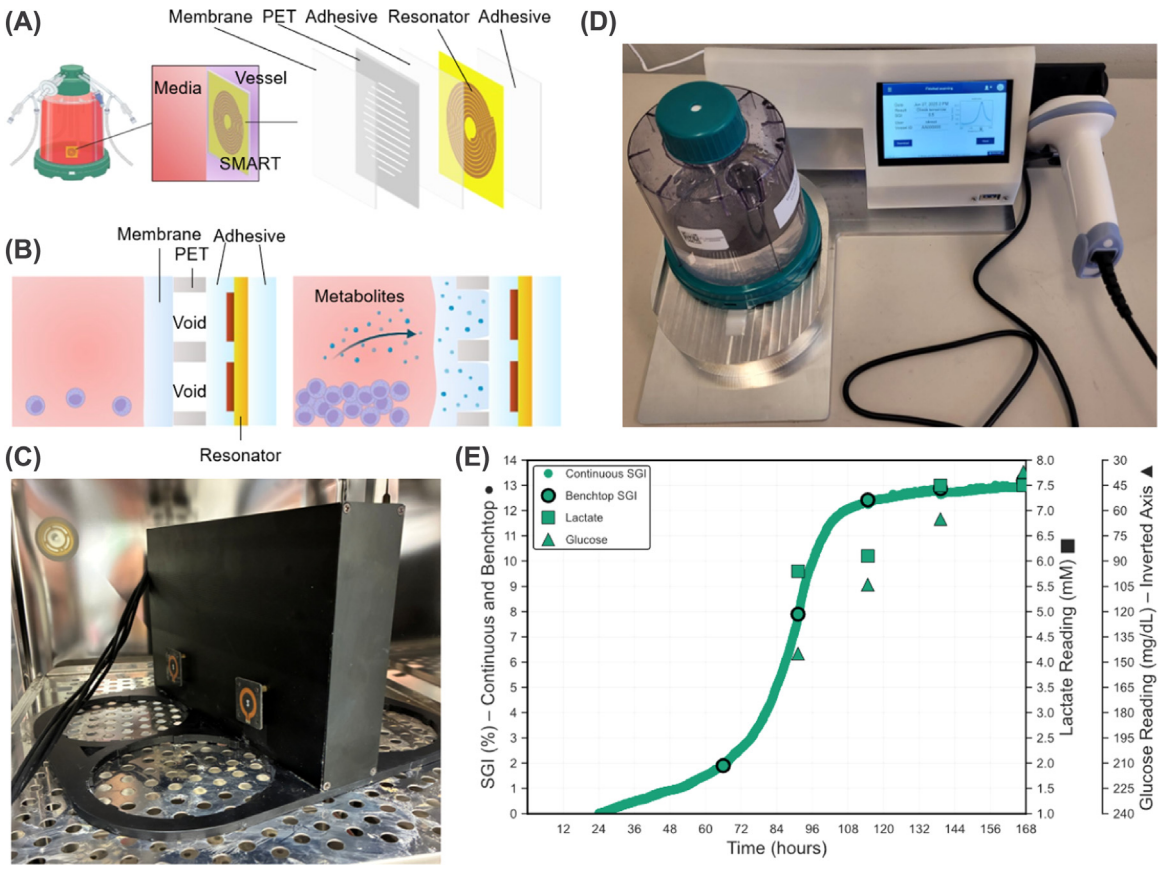

Fig. 2. SMART sensor structure and response. (A) The SMART sensor sticker is adhered to the inside of the G-Rex vessel to be in contact with the growth medium and is comprised of five layers (from fluid side: responsive membrane, PET sheet with engineered voids, adhesive tie layer, resonator, and adhesive layer for bonding to vessel interior. (B) Sensor transduction mechanism: as the cells secrete secondary metabolites (terpenoids) the membrane softens, fills the voids and the local permittivity to the resonant coil changes, causing a change in resonant frequency. (C) Custom reader to interrogate the sensors continuously within an incubator. (D) Custom reader to interrogate the sensors intermittently in a bench-top reader mode. In both cases, the G-Rex is kept closed and the cell layer is undisturbed. (E) Response of sensor reported as the change in resonant frequency from the start point (Skroot Growth Index, SGI) in both continuous and benchtop mode compared to traditional measures of glucose and lactate.

drop in cell count due to a temperature increase caused by the reader hardware. Hence, we settled on designing a custom-built reader that could wirelessly interrogate the resonant frequency of the sensor by performing frequency sweeps across a defined frequency range. Two reader configurations were implemented using the same core platform: 1) a continuous reader mode placed inside an incubator (Figure 2C), interrogating the sensor every 5 minutes, and 2) a bench-top reader mode (Figure 2D) in which the G-Rex was removed from the incubator, placed on the reader, and scanned for a single reading in under 30 seconds. The design and operation of the reader platform have been detailed in previous work [21].

Briefly, the reader applies a sinusoidal excitation (the frequency of the sinusoid can be digitally controlled) to an inductive loop that electromagnetically couples with the sensor, and the voltage measured across this loop yields a signal that exhibits a peak at the sensor's resonant frequency, which reflects changes in the sensor's local environment. This design improved on prior work to incorporate a larger frequency sweep range and advanced filtering of the output voltage signal.

Custom software was used to extract the resonant frequency from the voltage signal (Supplement 4). To reduce systematic error, a software-driven calibration step was performed using a reader-only measurement (with no sensor present) to account for the reader's intrinsic frequency response. The final sensor output was reported as the Skroot Growth Index (SGI; see Figure 2E), defined as the percentage change in resonant frequency from a predetermined equilibration time (e.g., 24 hours after the start of the run):

$$SGI(t) = 100 * \frac{f_R(t_{eq}) - f_R(t)}{f_R(t_{eq})} \quad (1)$$

where f_R denotes the sensor resonant frequency and t_{eq} represents the equilibration time. The use of a finite t_{eq} allowed for the elimination of any initial drift in sensor response caused by mechanical effects, ensuring that subsequent changes in SGI are primarily driven by biological phenomena.

3. Cell experiments—To validate the sensor response for use in a G-Rex based CAR-T manufacturing process, extensive cell culture testing was done at CellReady, LLC using cryopreserved Peripheral Blood Mononuclear Cells (PBMCs) as the starting material. To evaluate the sensors' ability to track cell growth for different growth profiles indicative of biological differences, three standard growth conditions were established by varying the seeding density: fast (200 million activated cells), medium (50 million activated cells), and slow (20 million activated cells).

   Healthy donor bulk leukapheresis product was purchased from Gulf Coast Blood. The leukapheresis product was collected under IRB approved protocols. Upon delivery to CellReady, the Leukapheresis product was stored overnight in a standard refrigerator at 2-8°C. The leukapheresis was processed following CellReady's standard protocol for closed system washing and Peripheral Blood Mononuclear Cell (PBMCs) isolation using the LOVO cell processing instrument from Fresenius Kabi. Briefly, PBMCs were isolated and re-suspended in CS10 (Biolife Solutions Cryostor) at 50 million

cells/mL. Aliquots of 20 ml (1×10E+09) were then dosed into CS50 bags (Miltenyi Biotec) and cryopreserved in a controlled rate freezer followed by transfer to long term storage in liquid nitrogen freezers. To obtain activated cells, a frozen bag containing 20 mL of 1.0×10E+09 PBMCs prepared as described above, was removed from long term storage, thawed using a Plasmatherm, then diluted with approximately 180 mL of Human T Cell Media (BioTechne REF CCM0380GMP-1L) and centrifuged. After centrifugation, the cells were re-suspended in 200 mL of Human T Cell Media and counted to determine % recovery and viability. 40 μL of Benzonase (Millipore Sigma) was then added to the cells and mixed, and the entire volume of cells and media was then transferred to a G-Rex 500M (Wilson Wolf REF G285500-RU) and brought to a total volume of 1000 mL for a 4-hour rest period in a standard CO2 incubator. After the 4-hour rest period the cells were −resuspended by gently rocking the G-Rex 500M and cells were activated by adding soluble CD3 (0.2 μg/mL) and CD28 (1.0 μg/mL) antibodies (ThermoFisher) to the G-Rex 500M which was then placed back into a standard cell culture incubator for 48-72 hours. This activation step allowed the creation of a bulk quantity of activated cells to be used in the SMART sensor experiments thereby isolating the activation step from experimental variables. After activation, a cell count of the activated cells is obtained and subsequently, activated cells were seeded into G-Rex 100M devices according to the assigned growth condition and topped up with 1 L of media with complete T cell media having 5% HAB Serum (BioIVT), IL7 and IL 15 at 10 ng/mL (BioTechne). Reader measurements were initiated upon activated cell seeding and cells were allowed to expand for a predetermined period ranging from 4 to 8 days.

Standard reference measurements of glucose and lactate were also performed on a daily basis starting 4 days after seeding. Each vessel was carefully opened in a sterile environment and a 100 μL sample was removed from the top without disturbing the cells. The sample was subsequently transferred to a microcentrifuge tube and gently inverted to mix, after which test strips were used with handheld meters. ForaCare Inc. FORA G20 Blood Glucose Monitor was used for glucose measurements whereas Hearts Bio Inc. Heartscare C1 lactate meter and Nova Biomedical Lactate Plus meters were used for lactate measurements. Upon conclusion of each cell culture run, the cells were harvested, and the total cell count, and final cell viability were assessed using a Cellometer K2 Fluorescent Cell Counter by Nexcelom (now a part of Revvity).

4. Data Collection and Harvest algorithm—Based on the data provided by the reader, SGI from the equilibration time (corresponding to SGI = 0) was determined by the software. In the case of the continuous read, this was done by referencing the preset equilibration time. In benchtop mode, the vessel was tracked by a unique identifier (barcode) allowing comparison between scan points. The software allowed for tracking the change in SGI at each data point, determining when the sensor response slowed and eventually plateaued. This plateau point was then used to correlate to cell growth data to determine trigger points for harvesting messaging.

Results and Discussion

Sensor performance

Initial testing of the sensor in continuous reader mode used a MetroVNA [22] as the reader hardware. It showed marked changes in cell production versus control vessels. Upon inspection, increased condensation was observed in the continuous read vessels and confirmed by temperature monitoring that indeed the continuous reader had raised the G-Rex temperature by ∼1°C, adversely affecting cell growth rate (Supplement 5). This was overcome by custom-designing the reader with special attention to power consumption of selected electronics parts and programming it to enter sleep mode between measurements, thereby reducing the overall heat generation and maintaining a lower board temperature. Using this cooler hardware, no statistically significant difference in final cell count and viability was observed among vessels with a sensor measured using cooler hardware, vessels with a sensor not measured by any hardware, and control vessels without a sensor (Supplement 5)—no pairwise comparisons between device groups were significant after Bonferroni correction (all adjusted $p = 1.00$).

Sensor-to-sensor consistency was assessed by comparing the response of four replicate sensors placed on the same vessel. All four sensors were placed radially along the interior wall of the G-Rex at the same vertical height, ensuring equal access to metabolites in the culture, which is mixed naturally via convection. Because SGI is a derived metric, the underlying measured resonant frequencies were used to quantify consistency via the coefficient of variation (CV) across the full duration of the experiment. For each frequency scan, CV was calculated as the standard deviation divided by the mean of the four sensors [23], expressed as a percentage. Figure 3A–C. show the SGI, measured resonant frequency, and corresponding CV of the four replicate sensors monitoring a CAR-T cell culture from an equilibration time of 24 hours to the end of experiment. The maximum CV remained below 1.25%, indicating high consistency across sensor replicates.

Having shown sensor consistency, we then evaluated the sensor capability to track different cell growth rates. This was done by seeding 3 independent G-Rex 100M vessels with activated cells from the same donor and the same activation source vessel at the same time with slow, medium, and fast growth conditions, respectively, and recording the sensor response for 7 days (168 hours). The sensor measurements were coupled with daily metabolite profiles in terms of lactate and glucose samples from each vessel, starting Day 4. The SGI data for the three conditions, using an equilibration time of 24 hours, is shown in Figure 3D, clearly highlighting the effectiveness of the sensors in differentially tracking the three growth conditions. It is evident from the correlation between the SGI curves and the lactate and glucose trends that the SGI tracks actual cell growth patterns inside the vessels. Additionally, it was found that the time taken to collect manual sampling parameters for 11 vessels by a GMP specialist was 29 minutes 34 seconds, whereas benchtop reader scans for the same vessels took 14 minutes 45 seconds—resulting in a time-saving of 50% with more improvements possible through software optimization.

We also evaluated the SMART sensor response using donor-derived selected T cells seeded (100×10^6 seeding density), activated, and expanded using the standardized G-CART^{TM} process. In this protocol, cell expansion (and hence reader measurements) started on Day 3 after a 3-day activation-phase from Day 0 and continued through Day 7. A negative control was run in parallel using the same seeding density and donor cells but with the activation agent and IL-15 cytokine omitted to intentionally stunt cell growth. As shown in Figure 3E, the SMART sensor selectively responded to active cell growth in the regular culture (3.61×10^9 viable cells upon Day 7 harvest) instead of the mere presence of cells in the negative control which only yielded 9.94×10^7 viable cells on Day 7.

Further testing was done to validate sensor response across various cell and vessel types. The Skroot sensor platform proved capable of successfully tracking both bacteria and mammalian cell growth across static and dynamic systems (Supplement 6). Moreover, the sensors demonstrated the ability to readily detect aberrant cell growth patterns. For instance, the presence of biological contaminants in a mammalian cell culture resulted in a markedly accelerated increase in SGI, consistent with the rapid expansion of the contaminants relative to the intended cells (Supplement 6).

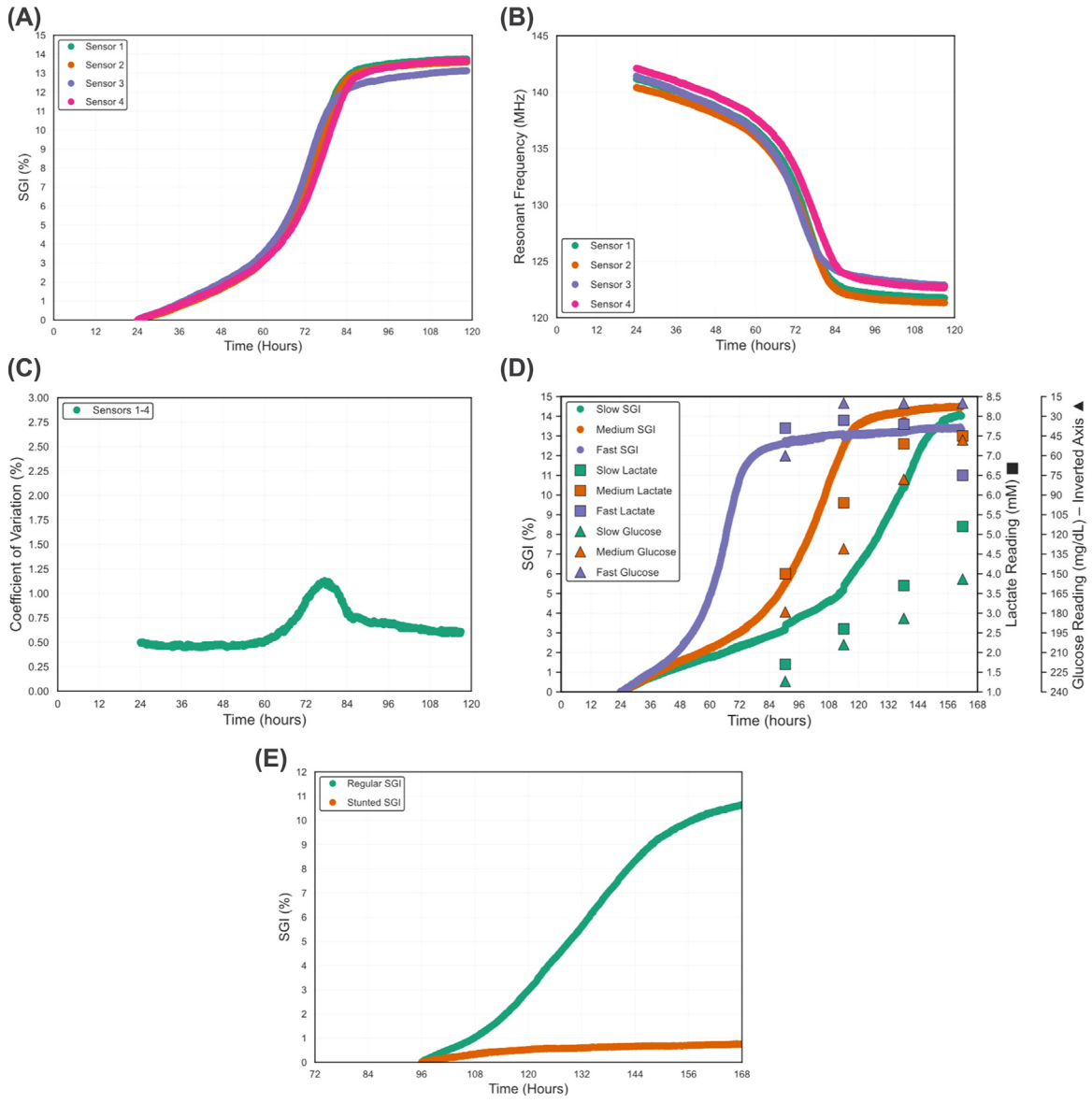

Fig. 3. (A) SMART sensor response (Skroot Growth Index—SGI) over time for one G-Rex 100M device with 4 replicate sensors, (B) Corresponding measured resonant frequency data, (C) Consistency among the 4 sensors expressed as coefficient of variation (CV) in measured resonant frequency, (D) SMART sensor response (Skroot Growth Index—SGI) over time for G-Rex 100M devices seeded under slow, medium, and fast growth conditions, alongside manually sampled lactate and glucose measurements. The sensor reliably distinguishes between different cell growth rates, as evidenced by distinct SGI trajectories and correlated metabolite profiles. (E) SMART sensor response comparing cell cultures seeded with an equal number of cells from the same donor cultured under regular activation condition versus a stunted condition, achieved by omitting the activation agent and the IL-15 cytokine—demonstrating that the SMART sensor selectively responds to active cell growth rather than the mere presence of cells.

Terminal cell count—verifying sufficient expansion prior to cryostorage

In standard CAR-T manufacturing, after expansion the cells are counted to verify sufficient dose quantity and viability prior to cryopreservation. The cells are then concentrated and re-suspended in bulk at the concentration specified on the label in the final drug product formulation media including a cryo-preservative and usually some type of Multiple Electrolytes for Injection, Type 1 Solutions, the bulk formulated drug product is then aliquoted into the primary drug product container, which is usually a ethylene-vinyl acetate (EVA) or polyolefin bags and then stored in vapor phase of liquid nitrogen. It is important to note that manufacturers often over-fill primary containers to compensate for the expected loss of cells due to the cryopreservation and thawing process.

Although postexpansion cell counts currently serve as the industry standard for formulating cell therapies at a target concentration, all counting methods inherently carry some degree of variance in total cell counts and recoveries—variability that is widely accepted across the field. Thus, a surrogate technique with a validated variance equal to or smaller than this accepted range could serve as the basis for drug-product formulation. It may be beneficial in some applications to allow a defined dose range on the label, provided a confirmatory count on a thawed sample of the finished product is recorded on the Certificate of Analysis (CoA) with the other quality-control (QC) data.

Taking this concept further, if a manufacturing process generates sufficiently repeatable yields, then formulation processes could be completely standardized on a per-process basis, eliminating the need for operator- or instrument-specific volumetric adjustments. For instance, if the manufacturing process can be validated to generate between 3.0×10^9 and 4.0×10^9 total cells in 95% of manufacturing runs, independent of donor starting material, and the SMART sensor can verify that the cell count would fall within this range, then conceivably all the necessary wash buffers and formulation medias could

be batch prepared for off the shelf formulation and fill. This approach would greatly simplify formulation, increase throughput, and shorten the interval from harvest to freezing, thereby enhancing process repeatability and improving post-thaw recovery and viability.

The correlation of final SGI saturation levels to final cell counts was investigated to explore the feasibility of this concept and determine if this measure could be used reliably to remove the necessity of the post expansion cell count prior to final formulation. We pooled data from 45 sensors that were all seeded at the same cell density (50 million activated cells) but from different donors and were run past SGI saturation. When plotting the final SGI to total viable cells (Figure 4A), there was a weak positive correlation (0.49 Pearson correlation coefficient). This analysis was confounded by the inherent variability of optical-based cell counters whose measurements are acknowledged to exhibit coefficients of variation (CV) ranging from 3% to 15% [24] We also assessed the distribution of final SGI (histogram plotted in Figure 4B–C) and observed a Weibull distribution shape. Most sensors saturated at > 9% SGI for this cell manufacturing process; however, there were a few (n = 3) that had a lower saturation point. By fitting the distributions of the sensor saturation points and the final viable cell counts (histogram and uniform distribution plotted in Figure 4D), we could confirm with 99% confidence that a final SGI > 7.08% corresponds to greater than 3.02 billion cells or a > 60X expansion. Additionally, in vessels where cell growth was intentionally stunted (see DMSO vessels in Supplement 7), SGI saturated at much lower values.

This resulting confidence may be sufficient to eliminate the post expansion cell verification count and simply formulate cells with off the shelf batch prepared formulation reagents and aliquot the harvested cells into five cryopreservation bags (> 600M cells per bag). One of the formulated and finished bags could then be used as the QC verification for final product QC testing, including cell count and viability measurements. If these parameters fall within the labeled range, and all other QC criteria are met, the remaining drug product bags may be released for patient administration. A major advantage of this approach is that it enables QC procedures to be staged and scheduled like a production line, ensuring that all product testing is performed on a representative finished drug product while enabling parallel QC operations on multiple drug product lots. The main caveat is that this methodology requires that the manufacturing process always produces an excess of product. However, given that the dose requirements for the currently approved CAR-T products range from 2×10^8 to 6×10^8 viable CAR+ cells, generating sufficient surplus should be feasible [25]. A standardized G-Rex 100M-CS process will produce greater than 2.0×10^9 CAR+ T cells.

Harvest indicator

After confirming the SMART sensor's ability to track cell growth and investigating how final SGI related with terminal cell count, we evaluated its potential to generate actionable insights by identifying harvest readiness of a cell culture. The objective of determining harvest readiness is to collect cells at peak viable count, which typically occurs during a window shortly after the exponential growth phase. Harvesting too early could result in suboptimal yield, while harvesting too late can lead to a decline in viability as cells begin to die and

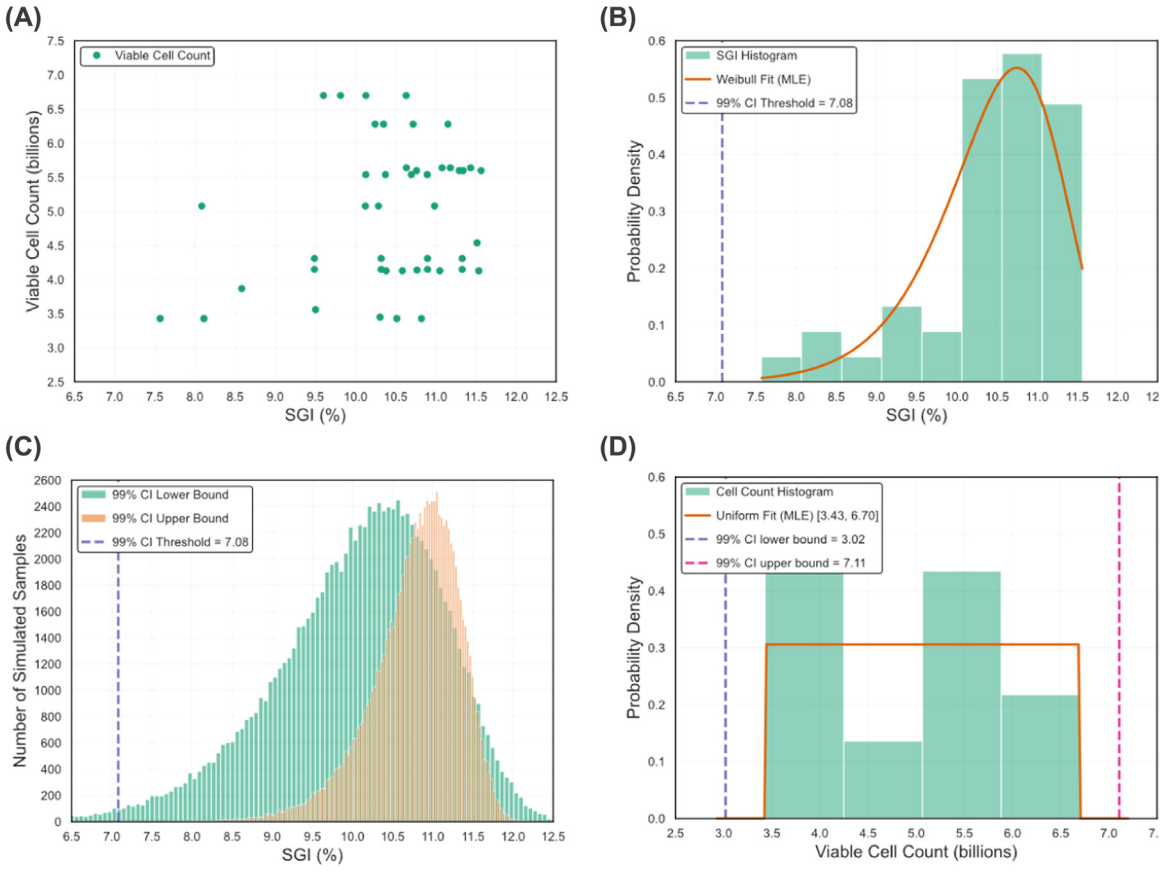

Fig. 4. (A) Correlation of total viable cells to final SGI measurement for 45 samples seeded with medium growth condition (50 million cells) exhibiting a weak positive correlation, (B) Histogram of final SGI values for samples overlaid with maximum-likelihood Weibull fit - the dashed purple line marks the 1 % lower–tail quantile (99 % confidence threshold of 7.08%). (C) Overlaid histograms of 100 000 simulated SGI draws using the lower– and upper–bounds of the 99% confidence interval (CI) on the Weibull parameters. The dashed purple line indicates the 99% "noise–floor" threshold from panel, (D) Histogram of viable cell counts with maximum-likelihood uniform fit spanning the observed min/max [3.43, 6.70] billion. Dashed purple and pink lines show the analytically derived 99 % CI lower (3.02 billion) and upper (7.11 billion) bounds.

the overall culture health deteriorates. Due to inherent biological variability of reviving frozen cells as well as varying quality of patient cells, the timing of this harvest window is difficult to predict *a priori*. Therefore, a real-time, sensor-based indicator of harvest readiness would be a valuable tool for improving process consistency and maximizing product quality.

To develop such an indicator, we designed an experiment in which three G-Rex devices were seeded identically with the medium growth condition (50 million cells) on the same day and harvested on Days 5, 6, and 7 postseeding. Sensor responses from all three vessels were monitored continuously, and the viable cell count from each vessel was assessed upon harvest (Figure 5A). The cell count results show that the Day 5 and Day 6 harvests were premature, yielding less than two-thirds the viable cell count achieved with the Day 7 harvest.

To compare the utility of continuous and benchtop reader modes for harvest decision-making, discrete points from the continuous SGI curves were sampled at each harvest time to serve as proxies for benchtop measurements (Fig. 5a). This approach is valid as both reader modes use the same underlying operating mechanism, and benchtop reader measurements indeed correspond to discrete samples on the continuous SGI curve (see Figure 2E). Additional benchtop

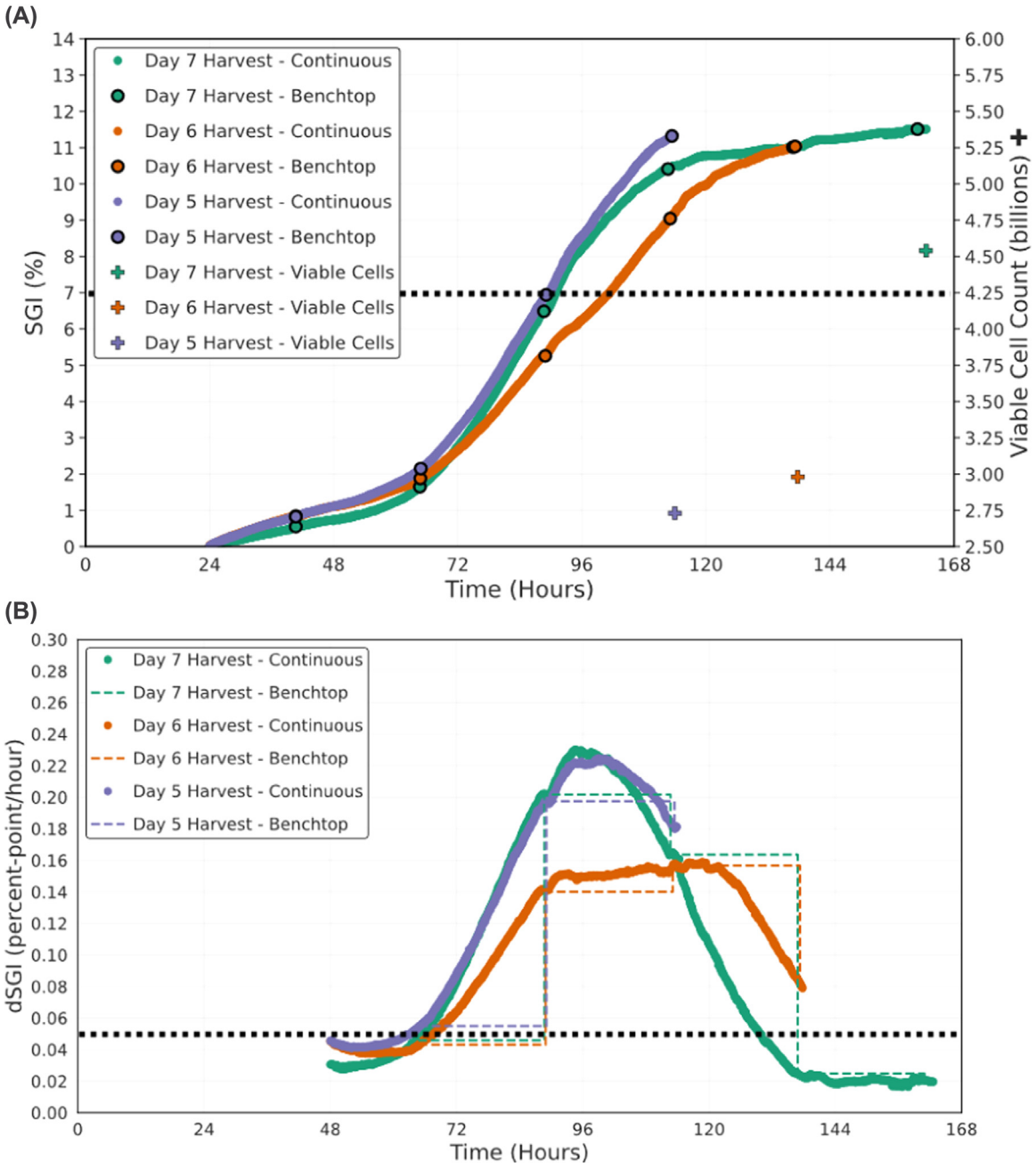

Fig. 5. (A) SMART sensor response (Skroot Growth Index—SGI) over time for three G-Rex 100M devices seeded identically with medium growth condition and harvested on three separate days (Day 5, 6, and 7 from seeding). The right Y axis denotes the viable cell count at the time of harvest for each vessel. Discrete data points (black-circled markers) represent benchtop proxy measurements sampled from the continuous SGI curve. The dotted dashed black line denotes the threshold which final SGI needs to cross to have a viable cell count greater than 3 billion. (B) The rate of change of SGI (dSGI) for the continuous measurements and the benchtop proxy. A binary harvest decision rule on dSGI activated upon SGI crossing 7 and using a threshold of 0.05 percent-point/hour for dSGI (dashed black horizontal line) would have indicated that the Day 5 Harvest and Day 6 Harvest vessels were not ready at the time of harvest, while the Day 7 Harvest vessel would have been identified as harvest-ready on Day 6. Notably, harvesting after dSGI dropped below the threshold resulted in a significantly higher viable cell count.

proxy measurements were generated at 24-hour intervals prior to the first harvest.

The numerical derivatives of both the continuous and benchtop SGI (denoted as dSGI) were computed for all three vessels (Figure 5B). While the continuous dSGI plots exhibited a bell-curve like response, the benchtop dSGI value exhibited expected stepwise behavior. After the SGI value crossed 7% (approximate SGI value beyond which saturation guarantees > 3 billion cells, see Figure 4), applying a binary decision rule with a threshold of 0.05 percentage points per hour for dSGI revealed that only the vessel harvested on Day 7 would have satisfied the criteria for harvest *a priori* (dSGI dropping below the dotted line threshold in Figure 5B)—demonstrating the potential utility of dSGI as a real-time harvest indicator. Therefore, users of the Skroot sensor system may perform application-specific cell culture runs to determine a suitable dSGI decision threshold for harvest readiness.

In our experiment, both the continuous and benchtop modes would have indicated that the manufacturing process was harvest ready approximately 24 hours prior to Day 7. The continuous dSGI crossed the dSGI threshold earlier as the benchtop dSGI was constrained by the discrete sampling intervals. Nonetheless, the ability of the benchtop reader to support harvest decisions with limited data is noteworthy enabling a simple yet effective "go/no-go" harvest indicator (Supplement 7). The specific threshold values of this harvest indicator are not expected to universally apply across different cell types, media formulations, or seeding and activation protocols. Therefore, we developed a simplified workflow to enable users to determine and tune application-specific harvest thresholds (Supplement 8).

The higher temporal resolution of continuous mode could further enable users to predict the onset of the harvest window further advance, thereby potentially enhancing the operational efficiency of the manufacturing process (Supplement 9).

Impact of SMART sensor on production costs and lean manufacturing

The sensors described herein directly affect the variable costs for each dose produced by reducing the amount of direct labor time of intermittent sampling (> 50% reduction per vessel), eliminating the need of an end cell count present in many use cases, and simplifying the measurement method enabling lower cost labor (or eventual automation). The sensors can also detect expansions that are not growing early for time-effective restarts. Unfortunately, such cost reductions will not significantly affect sticker price of these therapies until the industry is capable of achieving full scale production. Extreme overhead costs will continue to dominate the cost structure of producing these therapies and therefore variable costs are negligible (a subject of a forthcoming perspective article). At scale, which we aim to achieve with the G-Rex based manufacturing process, any improvement to the manufacturing process that 1) reduces the amount of direct labor time per drug product and 2) increases throughput on a given production line, will contribute to significant reduction in per dose costs. The SMART sensor has the potential to further augment G-Rex simplicity and scalability through a reduction in direct labor, while enhancing the manufacturer's ability to monitor and optimize the manufacturing process. Both readers can enable efficient review of past runs to determine points of inefficiency and be used to continuously perfect the manufacturing process, per LEAN manufacturing principles [26] that have been shown to reduce the cost of many goods we enjoy today (vehicles, computers, phones, etc.).

Conclusions

Herein, we have shown the application of the SMART sensor platform to the G-Rex production system for highly scalable, cost-effective production of cell and gene modified cell therapies. In this research, the sensor was optimized for scaled production and used in simulated clinical applications. It was validated with cytotoxicity testing, aging studies, and through demonstration with donor PBMCs. The cell work showed the ability to detect different growth rates, provide an indication for harvest timing, and the potential to eliminate the need of a cell count prior to cryostorage of drug product. We also demonstrated the reliability of this method as a surrogate measure for cell counting and periodic metabolite measurements thereby establishing its utility in eliminating periodic sampling for those applications that may require it while providing an option for continuous monitoring of cell expansion for G-Rex applications where this feature may be of use. Beyond the adoption of these new sensor systems, this work also presents a compelling call to continue standardizing and improving highly scalable parallel production methods, the central focus of G-Rex based cell therapy manufacturing.

Declaration of competing interests

The SMART G-Rex and accompanying reader are currently being developed as a commercial product to be sold through Wilson Wolf Manufacturing LLC. The author team hold patents in G-Rex and SMART sensors and readers.

Funding

This work was supported in part by National Science Foundation SBIR Grant Award# 2025552.

Acknowledgments

We would like to thank Eric Smith for early discussions on the SMART G-Rex concept.

Supplementary materials

Supplementary material associated with this article can be found in the online version at doi:10.1016/j.jcyt.2025.102034.

Article History:

Received 17 September 2025
Accepted 19 December 2025

References

[1] Fayyaz A, Haqqi A, Khan R, Irfan M, Khan K, Reiner Ž, et al. Revolutionizing cancer treatment: the rise of personalized immunotherapies. Discov Oncol 2024;15:756. https://doi.org/10.1007/s12672-024-01638-1.
[2] Zugasti I, Espinosa-Aroca Lady, Fidyt K, Mulens-Arias V, Diaz-Beya M, Juan M, et al. CAR-T cell therapy for cancer: current challenges and future directions. Sig Transduct Target Ther 2025;10:210. https://doi.org/10.1038/s41392-025-02269-w.
[3] Wang V, Gauthier M, Decot V, Reppel L, Bensoussan D. Systematic review on CAR-T cell clinical trials up to 2022. Cancers (Basel) 2023;15:1003. https://doi.org/10.3390/cancers15041003.
[4] Mikulic M. Estimated addressable patient population for CAR-T cell therapies worldwide as of 2019. Statista; 2022. https://www.statista.com/statistics/1098463/global-addressable-patient-population-car-t-cell-therapies-estimate/ (accessed September 1, 2025).
[5] Pagliarulo N. Novartis still hasn't solved its CAR-T manufacturing issues. BioPharma Dive. 2019 Dec 11. https://www.biopharmadive.com/news/novartis-kymriah-car-t-manufacturing-difficulties-cell-viability/568830/ (accessed September 1, 2025).
[6] Stanton D. Lonza: CAR-T manufacturing glitch an industry problem, not just Novartis's. BioProcess International. 2018 Jul 30. https://www.bioprocessintl.com/therapeutic-class/lonza-car-t-manufacturing-glitch-an-industry-problem-not-just-novartis-s (accessed September 1, 2025).
[7] Liu A. J&J, Legend's myeloma CAR-T Carvykti not slowing down in the face of new bispecific: Legend exec | Fierce Pharma 2023. https://www.fiercepharma.com/pharma/jjs-bispecific-not-slowing-car-t-down-carvykti-gets-fda-regular-review-earlier-myeloma [accessed 01.09.25].
[8] Nelson M. J&J halts Carvykti UK launch but is manufacturing to blame? BioProcess International (BioProcess Insider). 2023 Mar 21. https://www.bioprocessintl.com/global-markets/j-j-halts-carvykti-uk-launch-but-is-manufacturing-to-blame- (accessed September 1, 2025).

[9] Ayala Ceja M, Khericha M, Harris CM, Puig-Saus C, Chen YY. CAR-T cell manufacturing: Major process parameters and next-generation strategies. J Exp Med 2024;221:e20230903. https://doi.org/10.1084/jem.20230903.
[10] Ludwig J, Hirschel M. Methods and process optimization for large-scale CAR T expansion using the G-Rex cell culture platform. Methods Mol Biol 2020;2086:165–77. https://doi.org/10.1007/978-1-0716-0146-4_12.
[11] Kay Bates M, Fick D, Schneider J, Welch D, Ludwig J. G-Rex bioreactors incubated in Heracell™ Vios™ CR CO2 Incubators help prevent cross contamination and bacterial contamination in cell and gene modified cell therapy production. Cell Gene Ther Insights 2024;10:593–607. https://doi.org/10.18609/cgti.2024.072.
[12] Ran T, Eichmüller SB, Schmidt P, Schlander M. Cost of decentralized CAR T-cell production in an academic nonprofit setting. Int J Cancer 2020;147:3438–45. https://doi.org/10.1002/ijc.33156.
[13] Gotti E, Tettamanti S, Zaninelli S, Cuofano C, Cattaneo I, Rotiroti MC, et al. Optimization of therapeutic T cell expansion in G-Rex device and applicability to large-scale production for clinical use. Cytotherapy 2022;24:334–43. https://doi.org/10.1016/j.jcyt.2021.11.004.
[14] Ramos C, Alvarado C, Santana D, Siddiqui M, Miller B, Mueller A, et al. Real-time glucose/lactate monitoring using integrated maven sensors in G-Rex bioreactors for manufacturing of car-t cells. Cytotherapy 2025;27:S154. https://doi.org/10.1016/j.jcyt.2025.03.306.
[15] Huang QA, Dong L, Wang LF. LC passive wireless sensors toward a wireless sensing platform: status, prospects, and challenges. J Microelectromechanical Syst 2016;25:822–41. https://doi.org/10.1109/JMEMS.2016.2602298.
[16] Carr AR, Chan YJ, Reuel NF. Contact-free, passive, electromagnetic resonant sensors for enclosed biomedical applications: a perspective on opportunities and challenges. ACS Sens 2023;8:943–55. https://doi.org/10.1021/acssensors.2c02552.
[17] Chan YJ, Dileep D, Rothstein SM, Cochran EW, Reuel NF. Single-use, metabolite absorbing, resonant transducer (SMART) culture vessels for label-free, continuous cell culture progression monitoring. Adv Sci 2024;11:2401260. https://doi.org/10.1002/advs.202401260.
[18] Reuel NF, Chan YJ. Signal enhancement of resonant sensor for cell measurements. World Intellectual Property Organization patent WO2024058838 A1. 2024.
[19] Nicolaou A, Mauro C, Urquhart P, Marelli-Berg F. Polyunsaturated fatty acid-derived lipid mediators and T cell function. Front Immunol 2014;5:75. https://doi.org/10.3389/fimmu.2014.00075.
[20] Eastman Chemical Company. Accelerated aging in medical devices and packaging (SP-MBS-2021). Kingsport, TN: Eastman Chemical Company; 2021.
[21] Roy S, Chan YJ, Reuel NF, Neihart NM. Low-cost portable readout system design for inductively coupled resonant sensors. IEEE Trans Instrum Meas 2022;71:1–13. https://doi.org/10.1109/TIM.2022.3173277.
[22] metrovna. METROVNA DELUXE 250MHz. Metropwr 2015. https://www.metropwr.com/description/ [accessed 22.09.25].
[23] Shechtman O. The coefficient of variation as an index of measurement reliability. In: Doi SAR, Williams GM, eds. Methods of Clinical Epidemiology, Berlin, Heidelberg: Springer; 2013:39–49. https://doi.org/10.1007/978-3-642-37131-8_4.
[24] Richards C, Sarkar S, Kandell J, Snyder R, Lakshmipathy U. Assessing the suitability of cell counting methods during different stages of a cell processing workflow using an ISO 20391-2 guided study design and analysis. Front Bioeng Biotechnol 2023;11:1223227. https://doi.org/10.3389/fbioe.2023.1223227.
[25] van der Walle CF, Godbert S, Saito G, Azhari Z. Formulation considerations for autologous T cell drug products. Pharmaceutics 2021;13:1317. https://doi.org/10.3390/pharmaceutics13081317.
[26] Rocha L. Understanding lean manufacturing | KAIZEN Article 2024. https://kaizen.com/insights/understanding-lean-manufacturing-guide/ [accessed 22.09.25].